Urban heat islands and landscape heterogeneity: Linking spatiotemporal variations in surface temperatures to…

2 authors:

Alexander Buyantuyev
University at Albany, The State University of …
33 PUBLICATIONS **952** CITATIONS

SEE PROFILE

Jianguo Wu
Arizona State University
332 PUBLICATIONS **15,223** CITATIONS

SEE PROFILE

Some of the authors of this publication are also working on these related projects:

Project 12TH INTERNATIONAL LANDSCAPE CONFERENCE Russia, Tyumen, 21-27 August 2017 View project

RESEARCH ARTICLE

Urban heat islands and landscape heterogeneity: linking spatiotemporal variations in surface temperatures to land-cover and socioeconomic patterns

Alexander Buyantuyev · Jianguo Wu

Abstract The urban heat island (UHI) phenomenon is a common environmental problem in urban landscapes which affects both climatic and ecological processes. Here we examined the diurnal and seasonal characteristics of the Surface UHI in relation to land-cover properties in the Phoenix metropolitan region, located in the northern Sonoran desert, Arizona, USA. Surface temperature patterns derived from the Advanced Spaceborne Thermal Emission and Reflection Radiometer for two day-night pairs of imagery from the summer (June) and the autumn (October) seasons were analyzed. Although the urban core was generally warmer than the rest of the area (especially at night), no consistent trends were found along the urbanization gradient. October daytime data showed that most of the urbanized area acted as a heat sink. Temperature patterns also revealed intra-urban temperature differences that were as large as,

or even larger than, urban–rural differences. Regression analyses confirmed the important role of vegetation (daytime) and pavements (nighttime) in explaining spatio-temporal variation of surface temperatures. While these variables appear to be the main drivers of surface temperatures, their effects on surface temperatures are mediated considerably by humans as suggested by the high correlation between daytime temperatures and median family income. At night, however, the neighborhood socio-economic status was a much less controlling factor of surface temperatures. Finally, this study utilized geographically weighted regression which accounts for spatially varying relationships, and as such it is a more appropriate analytical framework for conducting research involving multiple spatial data layers with autocorrelated structures.

Keywords Urbanization · Surface temperature · Surface urban heat island · Land cover · Geographically weighted regression

A. Buyantuyev · J. Wu
School of Life Sciences, Arizona State University,
P.O. Box 874501, Tempe, AZ 85287-4501, USA

A. Buyantuyev · J. Wu
Global Institute of Sustainability, Arizona State
University, P.O. Box 874501, Tempe,
AZ 85287-4501, USA

A. Buyantuyev (✉) · J. Wu
Sino-US Center for Conservation, Energy, and
Sustainability Science (SUCCESS), Inner Mongolia
University, 010021 Hohhot, China
e-mail: a_buyant@hotmail.com

Introduction

Despite differences in regional climates, cities world-wide have developed one common characteristic—the urban heat island (UHI), i.e., urban areas have higher air and surface temperatures than their rural surroundings (Arnfield 2003; Oke 1982, 1997; Voogt

2002). UHI occurs as a result of land-cover transformations, mainly the replacement of natural vegetation and agricultural lands by impervious surfaces (concrete, asphalt, roof tops, and building walls) associated with urban land uses. These changes modify near surface energy budgets by reducing evapotranspiration, mounting solar energy absorbing surfaces, and creating heat-trapping canyon-like urban morphology. Excessive heat in cities is continuously produced and emitted to the atmosphere by building infrastructure and transportation. Urban areas have become increasingly important drivers of local and regional climatic and environmental changes with many deleterious consequences for social and ecological processes (Bonan 2002; Wu 2008a, b). In arid and semi-arid climates UHIs exert extra heat stress on organisms, including humans. Located in the northern Sonoran desert and characterized by mild winters and hot summers, the Phoenix metropolitan region, USA has an average annual daily maximum temperature of 30°C. With rapid urbanization in this area during the last 50 years, the mean daily air temperature has increased by 3.1°C and nighttime minimum temperature by 5°C (Baker et al. 2002; Brazel et al. 2000). Summers in Phoenix are characterized by a peak in energy and residential water consumption (Baker et al. 2002; Guhathakurta and Gober 2007; Watkins et al. 2007). Understanding and quantifying UHI and its factors are important steps toward improving the quality of life of urbanites and achieving urban sustainability in Phoenix and other cities (Grimm et al. 2008; Wu 2008a).

It is important to recognize the multiplicity of UHIs, characterized by the scale of analysis, type of medium studied, and type of measurement instrumentation (Arnfield 2003). UHIs are commonly measured in terms of air temperatures analyzed at two scales—the urban canopy layer UHI and the urban boundary layer UHI (Oke 1976). Remote sensing made it possible to measure the upwelling thermal radiance, and this indirect measurement of surface, or skin, temperature is often referred to as the Surface UHI (SUHI) (Roth et al. 1989; Voogt and Oke 2003). Although UHI and SUHI tend to co-vary spatially and temporally, the associations between air and surface temperatures are not perfect and depend on many factors. Specifically, surface temperatures display a stronger dependence on microscale site characteristics than air temperatures (Arnfield 2003;

Nichol 1996). Studies of urban surface temperatures in the past two decades have advanced our understanding of spatial thermal patterns and their relation to surface characteristics (Balling and Brazel 1988, 1989; Gallo et al. 1993b; Jauregui 1993; Lu and Weng 2006; Nichol 1998; Owen et al. 1998b; Quattrochi and Ridd 1998; Roth et al. 1989; Streutker 2002; Weng et al. 2004; Wilson et al. 2003; Xian and Crane 2006), and elucidated urban surface energy budgets (Grimmond and Oke 2002; Grossman-Clarke et al. 2005; Hafner and Kidder 1999; Kato and Yamaguchi 2007; Kim 1992; Voogt and Grimmond 2000).

Both UHI and SUHI develop primarily at night throughout a year, and depend heavily on weather conditions (Arnfield 2003; Souch and Grimmond 2006). The intensity of UHI in arid and semi-arid environments is found to change seasonally due to the high variability in vegetation (Jonsson 2004). It is generally more intense during dry seasons when leafless canopies and the dry and bright soil increase the albedo. Reduced thermal heat capacity (lower heat absorption) and more effective radiative cooling of dry grounds increase the urban–rural temperature contrast. High similarities in surface characteristics between urban and rural landscapes (e.g., Kuwait City) lead to the lack of well-developed UHI (Nasrallah et al. 1990). Urban vegetation, however, moderates surrounding microclimates through increased latent heat exchange, shading, and lack of heat from combustion sources (Jonsson 2004; Spronken-Smith and Oke 1998). The influence of urban parks and greenspaces as cooling elements can extend in the order of hundreds of meters beyond their boundaries (Spronken-Smith and Oke 1998; Upmanis et al. 1998).

Although spatial patterns of UHI and SUHI and general characteristics of urban-to-rural temperature differences have been extensively studied, a comprehensive understanding of how the heterogeneity of land covers affects temperature distributions on multiple spatial scales is still lacking. Thus, the objectives of this study were twofold: (1) to quantify diurnal and seasonal surface temperature variations in the Phoenix metropolitan region at two spatial scales, and (2) to explore biophysical and socioeconomic factors that are responsible for the temperature variations. Previous studies found strong correlations between temperature and variables affecting its spatial and temporal variation at both fine (Hartz

et al. 2006; Stabler et al. 2005; Stefanov et al. 2004) and coarse scales (Balling and Brazel 1988, 1989; Brazel et al. 2007; Hsu 1984; Jenerette et al. 2007). Here we used spectral and thermal data from the Advanced Spaceborne Thermal Emission and Reflection Radiometer (ASTER) and auxiliary spatial GIS data to further investigate the temporal and spatial patterns of Phoenix's SUHI. Specifically, we examined urban–rural differences and intra-urban variability of surface temperatures using detailed land-cover information. We also explored SUHI drivers that were known to directly affect surface temperatures, including percent vegetative cover, percent impervious surface, presence of open water, topography, and land-cover heterogeneity. At the broader scale we aggregated to the level of available socio-economic data and used multiple regressions to assess their contribution to the explanation of observed temperature patterns.

Methods

ASTER data processing

We obtained atmospherically corrected level 2 ASTER data (Table 1) by using the search and retrieval tools provided by the Land Processes Distributed Active Archive Center (LP DAAC) of the US Geologic Survey (USGS). Pairs of daytime and nighttime data for hot and cold seasons were selected based on pre-defined criteria: (1) No precipitation for at least 4 days prior to imaging; (2) Relatively calm wind conditions; (3) Cloud-free conditions; (4) No more than 3 days between images in each day-night pair; (5) Maximal spatial overlap between all datasets. Data from the summer and late autumn of 2003 and consisting of atmospherically and topographically corrected VNIR-SWIR surface spectral reflectance (AST07, available for daytime only) and surface kinetic temperature (AST08, by special request) met these criteria. Summertime data were collected on June, 21 at 9:41 p.m. and June, 24 at 11:15 a.m. LST. Autumn data were collected on October, 20 and 21 at 9:35 p.m. and 11:21 a.m. LST, respectively. All images were subset to the area of common spatial overlap, centered on the city of Phoenix and extending 91 km in the north-south and 33 km in the west-east directions.

For each season we created land-cover maps following two steps. In the initial image classification we used the expert classification system (Stefanov et al. 2001) which performs a posteriori sorting of classes derived using the maximum likelihood classification. The system was developed for Landsat data in ERDAS Imagine 8.7. It applies a sequence of Boolean decision rules and uses information from auxiliary data layers including land-use map, normalized difference vegetation index (NDVI), water

Table 1 Characteristics of the ASTER multispectral instrument

Spectral subsystem	Band	Spectral range (μm)	Spatial resolution (m)
Visible—near infrared (VNIR)	1	0.52–0.60	15
	2	0.63–0.69	
	3 N (nadir view)	0.76–0.86	
	3B (backward scan)	0.76–0.86	
Shortwave—near infrared (SWIR)	4	1.60–1.70	30
	5	2.145–2.185	
	6	2.185–2.225	
	7	2.235–2.285	
	8	2.295–2.365	
	9	2.360–2.430	
Thermal infrared (TIR)	10	8.125–8.475	90
	11	8.475–8.825	
	12	8.925–9.275	
	13	10.25–10.95	
	14	10.95–11.65	

agricultural rights database, city boundaries, Native American reservation boundaries, and variance texture images computed by a 3 × 3 pixel moving window. We adapted the classification system to be used with ASTER VNIR-SWIR data and acquired contemporaneous auxiliary spatial layers. NDVI, which provides an estimate of the abundance of actively photosynthesizing vegetation (Huete and Jackson 1987; Tucker 1979), was computed as

$$NDVI = (NIR - RED)/(NIR + RED) \qquad (1)$$

where NIR corresponds to band 3 N and RED corresponds to band 2. The index is based on the property of green leaves to absorb wavelengths in the red zone and strongly reflect in the near-infrared zone of electromagnetic spectrum represented by values ranging from −1 to 1. Bands 2 and 3 N were also used to produce texture images. The second step was to merge this preliminary map with the Southwest Region GAP (SWReGAP) provisional land-cover classification (Lowry et al. 2005). Anthropogenic land covers were retained from the initial classification but localities outside incorporated areas were coded using natural vegetation categories from the SWReGAP map. The final land-cover maps, one for June (Fig. 1) and one for October, each has 15 categories and provide ecologically meaningful subdivision of the area.

Surface temperature images were produced using the temperature/emissivity separation hybrid approach developed by the ASTER science team. This method calculates temperature by means of Plank's Law using normalized emissivity of five thermal bands of ASTER and has the relative accuracy of ±0.3°C (Gillespie et al. 1998). Surface temperature images were spatially co-registered by using ground control points from the 0.6-m color aerial photography mosaic and applying a first order polynomial transformation.

Acquisition and processing of auxiliary spatial data

We obtained the 10-m digital elevation model (DEM) provided by the USGS and socio-economic geographic data compiled by the US Census Bureau. A group of variables derived from these sources was used to explore their statistical relationships with surface temperature. DEM was resampled to the resolution of ASTER and used to calculate slope and aspect grids. We used socio-economic data at the level of Census block group, a subdivision of the Census tract that represent the smallest geographic unit for which the desired information was available. Several variables hypothesized to affect surface temperature (Jenerette et al. 2007) were extracted from the Decennial Census 2000 including total population, population density, number of households, median household income, number of families, median family income, number of housing units, and median age of housing structures.

Statistical analyses

The magnitude and temporal variability of SUHI were analyzed by stratifying temperature grids across land-cover maps and computing descriptive statistics. Land cover is an integrative characteristic which was used to typify the urban–rural gradient with the major assumption of relative uniformity of surface temperature between pixels of a given land cover. To compare between land covers we sampled all temperature grids using a large subset ($n > 16,000$) of randomly chosen points spaced at no less than 300 m. This sampling design was chosen to minimize the effects of spatial autocorrelation and to meet independence assumption. Computed global Moran's I spatial autocorrelation indices (Fortin and Dale 2005) were 0.06 for June daytime and 0.17 for nighttime, and 0.04 for October daytime and 0.1 for nighttime, confirming spatial patterns of the four samples were close to random. We used the Tukey–Kramer HSD (Honestly Significant Difference) test for unequal group sizes to compare means calculated for each land cover (Neter et al. 1996).

Relationships between temperature, vegetation, surface characteristics, and socio-economics were investigated using traditional multiple ordinary least squares (OLS) regression and geographically weighted regression (GWR) (Fotheringham et al. 2002) focusing only on populated areas. To ensure all variables were analyzed at a commensurate scale we performed scale translation. We aggregated the data to the coarsest spatial resolution represented by the Census block groups ($n = 1,368$) for which demographic and economic characteristics were assumed homogenous. We derived spatial averages of NDVI, elevation, slope, aspect, and fractions of impervious

Fig. 1 June 2003 land cover map of Phoenix, Arizona produced from ASTER imagery
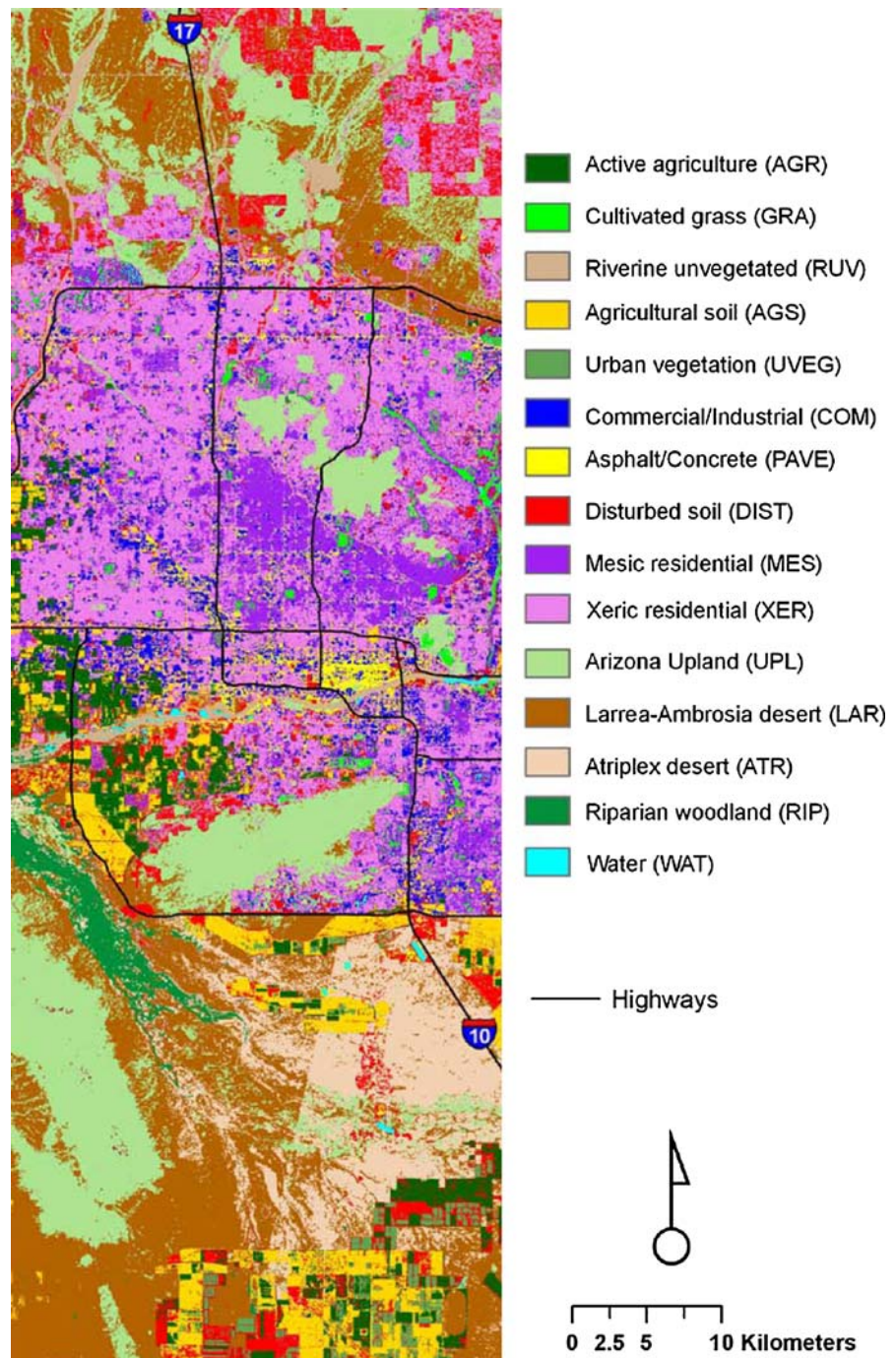
surfaces (i.e., buildings and pavements), paved area, and open water within each block group. Land-cover variability was assessed as the number of land-cover categories encountered in each block group. Final selection of the independent variables was obtained by stepwise forward and then stepwise backward

regressions. Bivariate regressions for temperature and the two best independent variables from each subset were constructed to describe the direction and strength of relationships.

Geographically weighted regression is based on the following interrelated principles: spatial data

often do not meet the assumption of stationarity; relationship estimation is affected by spatial structures of data; relationships between variables are not necessarily global (Fotheringham et al. 2002). To deal with these issues GWR redefines the standard OLS given by:

$$y_i = \beta_o + \beta_1 x_{i1} + \cdots + \beta_n x_{in} + \varepsilon_i \qquad (2)$$

where y_i is the dependent variable at point i; x_{i1} and x_{in} are independent variables at point i; β_o, β_1 and β_n are parameters to be estimated; and ε_i is the error term at point i. The GWR framework allows local rather than global parameters to be estimated and is rewritten as:

$$y_i = \beta_o(u_i, v_i) + \beta_1(u_i, v_i)x_{i1} + \cdots + \beta_n x_{in} + \varepsilon_i \quad (3)$$

where (u_i, v_i) denotes the coordinates of the ith data point and β_o and β_1 are continuous functions of (u, v) at point i (Fotheringham et al. 2002). The GWR software calculates a local equation at each data point where the contribution of a local sample is weighted based on the spatial proximity to the data point. Calibration of local models for our data used the adaptive Gaussian spatial kernel, which is more suited for data distributed unevenly in space. The weighting function for kernel bandwidth was based on minimization of the Akaike information criterion (AIC_c). GWR outputs parameter estimates for each local equation along with goodness-of-fit diagnostics including local versions of coefficient of determination and the residuals (Fotheringham et al. 2002). All statistical analyses other than GWR were performed using SAS JMP 7.0.2 software.

Results

Seasonal and diurnal characteristics of temperature variation across the Phoenix metropolitan region

Surface temperature maps (Fig. 2) illustrate spatial patterns and provide visual confirmation of association with land covers. The urban core around the Sky Harbor International airport along with major roads is warmer than the rest of the developed area during nighttime on both seasons. The majority of urban locations can be as warm as, or cooler than, the outside desert. The latter is particularly evident from
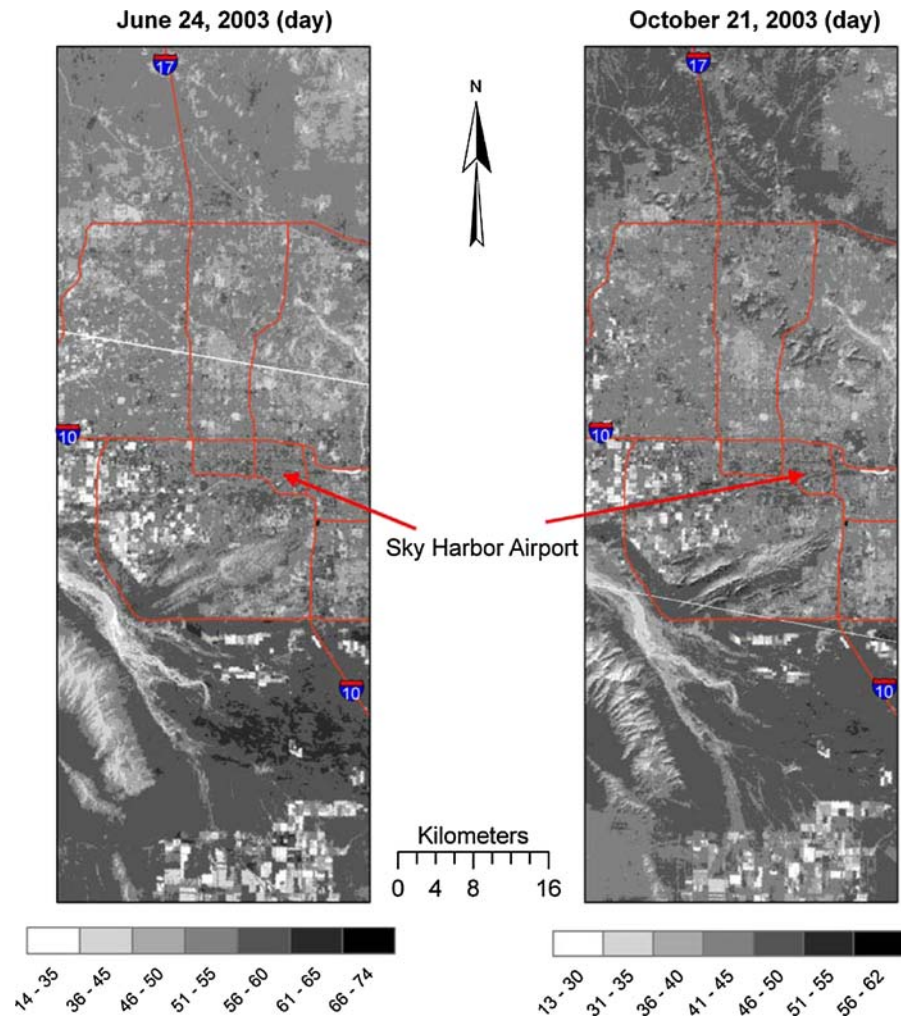
October daytime image when most of the urban and agricultural areas emerged as 'cool' patches rather than heat islands. Mountain slopes covered by Arizona Upland (UPL) communities are generally warm, but spatial patterns are very heterogeneous reflecting differences in slope, aspect and shading. Heavily vegetated areas, such as riparian woodlands and active croplands, are consistently cooler than other areas. Interestingly, the difference between riparian areas and other land covers is minimal in the June nighttime map. Larrea-Ambrosia desert (LAR) and Atriplex desert (ATR), characterized by the lowest vegetation density experienced the greatest day-night temperature difference at both seasons. Highly urbanized locations, desert mountain slopes, and agricultural fields are recognized as those with the least day-night difference (Fig. 3).

Spatially averaged temperatures provide further details on differences between land covers (Fig. 4). They corroborate the patterns observed in the temperature maps and quantify temperature gradients across the area. ATR and LAR were warmest during the daytime and experienced large amplitudes in daytime temperature transitions. They often formed statistically significant individual groups. Paved areas (PAVE) and commercial (COM) localities together with UPL and residential xeriscapes (XER) were the warmest land covers at night but occupied intermediate positions along the daytime temperature gradient. They frequently formed common groups with other land covers. Urban vegetation consisting of isolated dense patches of trees and shrubs was always a distinctive group with low temperatures. Riparian areas were also at the cool end of the gradient except for nighttime June. While the results suggested no consistency in spatial variation in temperature along the gradient of urbanization at both seasons, we did see distinct spatial patterns. The October daytime data showed that the urbanized area is a cool island (except fallow agriculture) with overall temperatures colder than that of the surrounding desert (Fig. 4).

Regression analyses of relationships between surface temperature and biophysical and socio-economic factors

Mean NDVI was the most significant explanatory variable of daytime surface temperature, but the correlation was notably weaker at night (Fig. 5).

Fig. 2 Surface temperature (°C) maps of Phoenix

June 24, 2003 (day)

October 21, 2003 (day)

N

Sky Harbor Airport

Kilometers

0   4   8   16

14 - 35   36 - 45   46 - 50   51 - 55   56 - 60   61 - 65   66 - 74

13 - 30   31 - 35   36 - 40   41 - 45   46 - 50   51 - 55   56 - 62

Unlike vegetation, fraction of paved area correlated positively with temperature. Although the relationship was not very strong, paved area played a major role in explaining night temperature patterns at both seasons (Fig. 5). Median family income was the second most important predictor of daytime temperatures. We estimated that for every NDVI increase by 0.1 (or roughly 10% cover) daytime mean temperature of block groups decreased by 2.8°C in June and 2.4°C in October. At night NDVI was approximately two times less efficient in decreasing temperature. Both summer and autumn nighttime surface temperatures increased by 0.9°C for each additional 10% increase in paved area within block groups. Finally, daytime temperatures decreased by 0.36°C in June and by 0.23°C in October for every $10,000 increase in family income.

Parameter estimates of the multiple regressions demonstrate that, in the multivariate framework, surface temperatures are always negatively related to vegetation, but the relationship of surface temperatures to other variables may change the sign (Table 2). For example, temperature was related to all other variables negatively in June and October daytime, but positively in October nighttime. Land-cover variability (LCVAR) and age of housing structures (YBUILT) changed to a negative relationship in June nighttime. Surface temperature did not appear to be related to YBUILT at both day and night in October and in June daytime. It was also not related to elevation (ELEV) in October daytime. Table 3 shows diagnostics and allows comparisons between the OLS and GWR. Both sets of models replicated data reasonably well with adjusted R^2

Fig. 2 continued
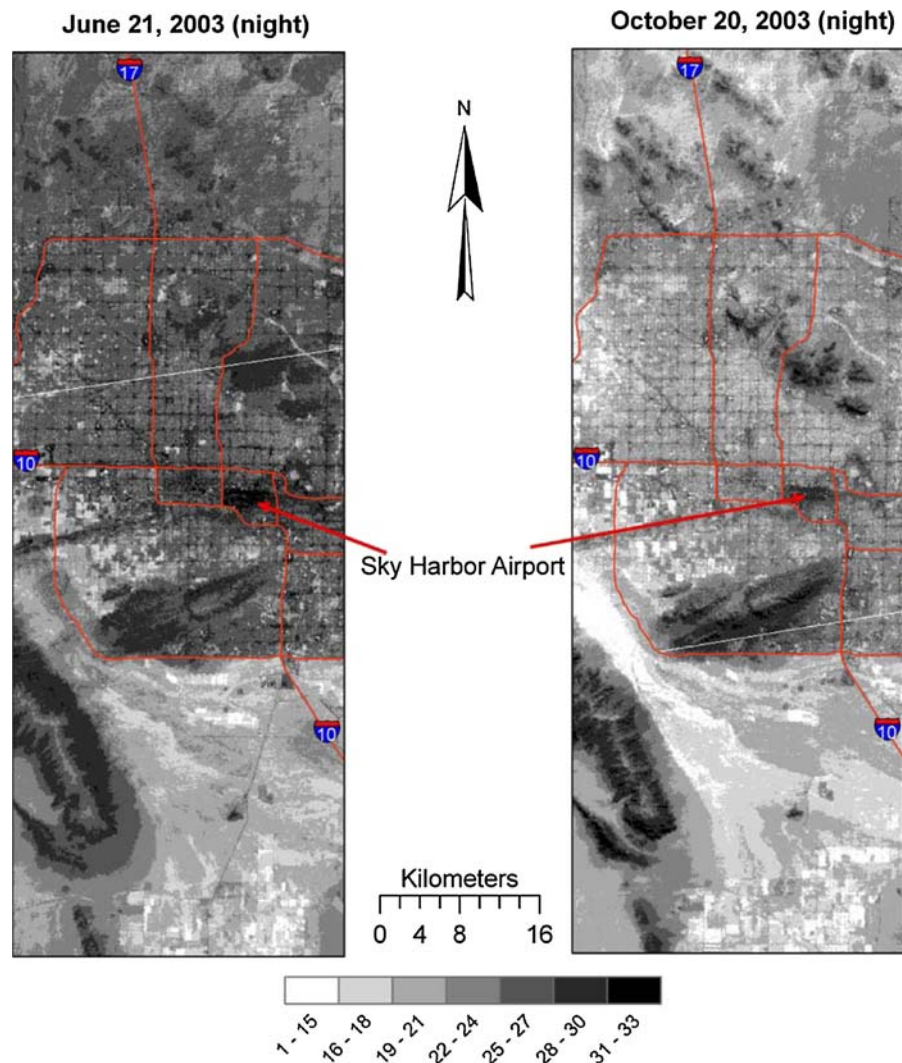
ranging from 0.39 to 0.59 for OLS and 0.61 to 0.77 for GWR. The GWR explained more variance in mean surface temperature than the OLS did although the increase is to be expected given the difference in degrees of freedom (Fotheringham et al. 2002). Other diagnostics also confirm that the GWR provides a considerable improvement over OLS regressions. It is indicated by consistently smaller AIC_c and standard error of GWR estimates. Additionally, the F test ($\alpha = 0.05$) of the significance of improvement suggested the GWR performed better in all cases. The difference is particularly large for October nighttime temperature prediction (Table 3). The general spatial patterns of mean surface temperatures for Census block groups

predicted by global OLS and GWR multiple regression models seem similar (Fig. 6), but differences do exist in the detail. Both GWR and OLS predict temporally stable and warmer cluster of block groups in the area around the Sky Harbor International Airport. Another heat cluster (except June daytime) is found near Camelback Mountain between Phoenix and Paradise Valley. However, OLS predictions for daytime show a significantly lower magnitude of these heat islands. This may be an indication of the ability of GWR in highlighting areas that are hot locally, but not depicted as such when modeled by the OLS. Similar discrepancies in predictions can be noticed in the cooler agricultural area in western Glendale.

Fig. 3 Day-night differences in surface temperature (°C) of Phoenix, AZ at two seasons
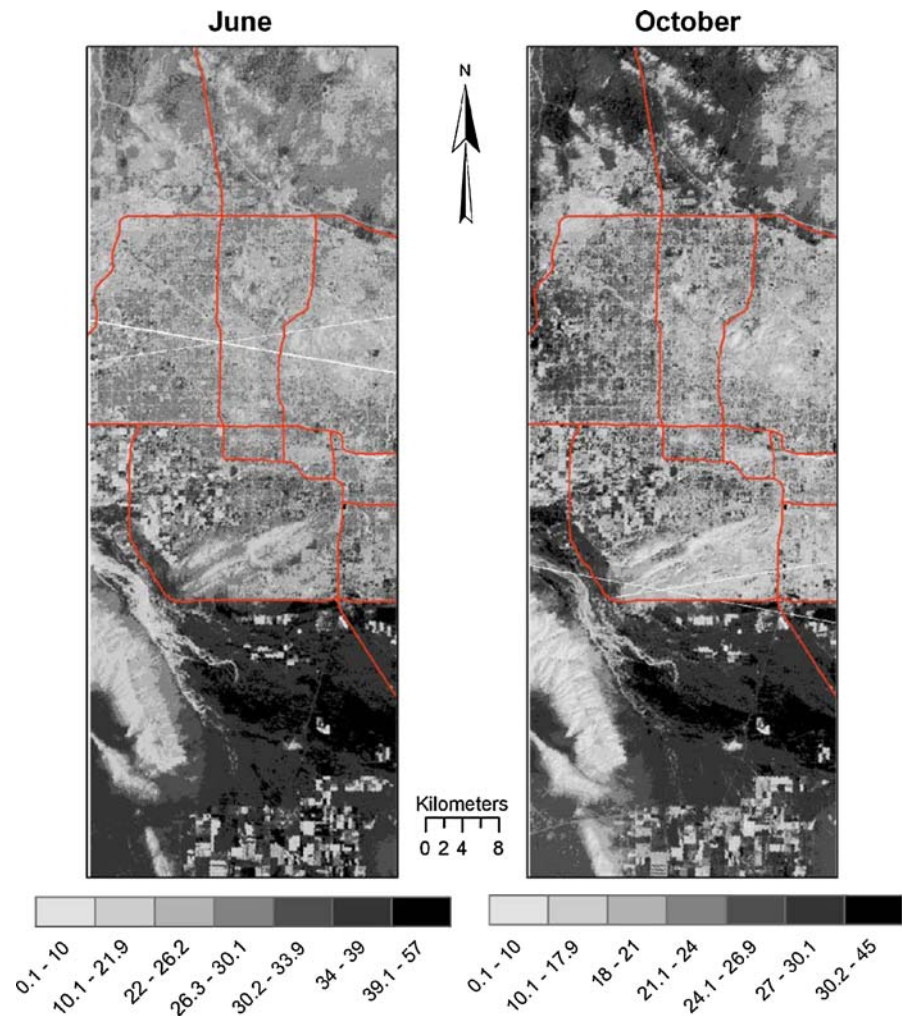
Discussion

Landscape ecology has much to offer for understanding the spatial pattern of surface temperatures along urbanization gradients on multiple scales, but the application of landscape ecological principles to the studies of UHI is still scarce (Weng and Larson 2005). Concepts and tools developed in landscape ecology can benefit the analysis of UHI formation, its scaling properties, and impacts on human health and comfort. The landscape ecological approach we employed in this study focused on diurnal and seasonal changes in spatial structure of surface temperatures in relation to urban landscape pattern. By examining these patterns along a landscape modification gradient, we have obtained a number of interesting findings.

Spatiotemporal patterns of SUHI at different scales

Both UHI and SUHI manifestation and their perception by organisms can change with the scale of analysis, as reported in previous studies (Arnfield 2003). The difference between the urban canopy and the urban boundary layers represents the important separation of local scale processes of energy exchange and air flows near the ground from those controlled by large scale processes (Oke 1976). Accordingly, we studied surface temperature patterns
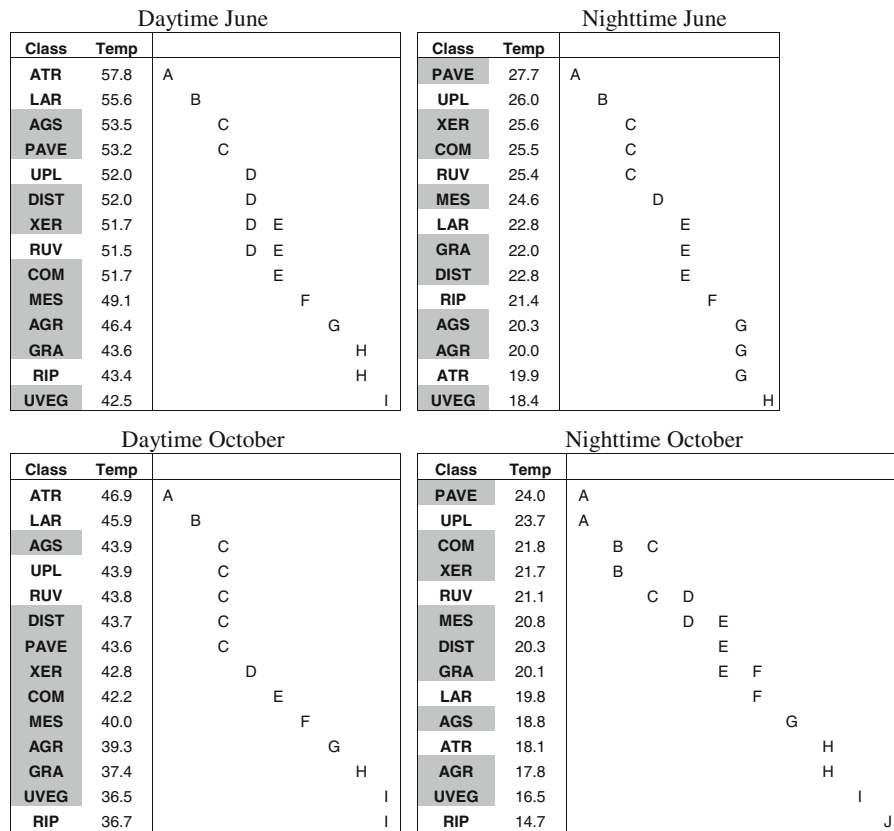
Daytime June

Class	Temp	A	B	C	D	E	F	G	H	I
ATR	57.8	A								
LAR	55.6		B							
AGS	53.5			C						
PAVE	53.2			C						
UPL	52.0				D					
DIST	52.0				D					
XER	51.7				D	E				
RUV	51.5				D	E				
COM	51.7					E				
MES	49.1						F			
AGR	46.4							G		
GRA	43.6								H	
RIP	43.4								H	
UVEG	42.5									I

Nighttime June

Class	Temp	A	B	C	D	E	F	G	H
PAVE	27.7	A							
UPL	26.0		B						
XER	25.6			C					
COM	25.5			C					
RUV	25.4			C					
MES	24.6				D				
LAR	22.8					E			
GRA	22.0					E			
DIST	22.8					E			
RIP	21.4						F		
AGS	20.3							G	
AGR	20.0							G	
ATR	19.9							G	
UVEG	18.4								H

Daytime October

Class	Temp	A	B	C	D	E	F	G	H	I
ATR	46.9	A								
LAR	45.9		B							
AGS	43.9			C						
UPL	43.9			C						
RUV	43.8			C						
DIST	43.7			C						
PAVE	43.6			C						
XER	42.8				D					
COM	42.2					E				
MES	40.0						F			
AGR	39.3							G		
GRA	37.4								H	
UVEG	36.5									I
RIP	36.7									I

Nighttime October

Class	Temp	A	B	C	D	E	F	G	H	I	J
PAVE	24.0	A									
UPL	23.7	A									
COM	21.8		B	C							
XER	21.7		B								
RUV	21.1			C	D						
MES	20.8				D	E					
DIST	20.3					E					
GRA	20.1					E	F				
LAR	19.8						F				
AGS	18.8							G			
ATR	18.1								H		
AGR	17.8								H		
UVEG	16.5									I	
RIP	14.7										J

Fig. 4 Groupings of land cover classes based on spatially averaged surface temperature at four time periods. Land cover codes are the same as in the land cover map legend in Fig. 1 (anthropogenic ones are *shaded* here). Significance of differences between the means was assessed by the Tukey procedure. *Letters A* through *J* represent statistically significant groups (at $\alpha = 0.05$) ranked by surface temperature. Classes not connected by same letter belong to different groups

at two scales. One scale corresponded to the original resolution of ASTER data, and the other focused on data aggregated to the level of block groups at which broader patterns were investigated by relating temperature to biophysical and socio-economic variables. This higher level is appropriate for understanding the impacts of excessive heating on human health and comfort (Ruddell et al. 2009). It provides valuable information for sustainable urban planning and better decision-making.

Analyses of diurnal and seasonal variations of surface temperature revealed the existence of nighttime SUHI and the daytime heat sink in Phoenix at both the early summer and the late autumn seasons. Formation of the morning heat sink is not unique to the arid Phoenix, and has been previously observed in cities located in other geographic settings (Nichol 1996; Pena 2008; Weng and Larson 2005). The heat sink has been attributed to a variety of causes, primarily high thermal inertia of built areas, shading by tall buildings, and moisture differences between urban and rural areas (Carnahan and Larson 1990; Oke 1976; Pena 2008). In Phoenix, all of these reasons, except shading by high-rise estates, are likely to contribute to the formation of the morning heat sink. The described temperature patterns were persistent at both scales (Figs. 2, 6). Although the coarser resolution approach enables consideration of socio-economic variables, it convolves variations in land cover because the analysis focuses on statistical properties of variables. Upscaling to this resolution required combining on average 3,300 NDVI pixels (15 m) or approximately 90 temperature pixels (90 m).

A number of researchers have described complex spatial patterns of satellite-derived surface temperature

Fig. 5 Scatter plots of bivariate relationships between surface temperature and its two most influential explanatory variables at each time period ($n = 1,368$)
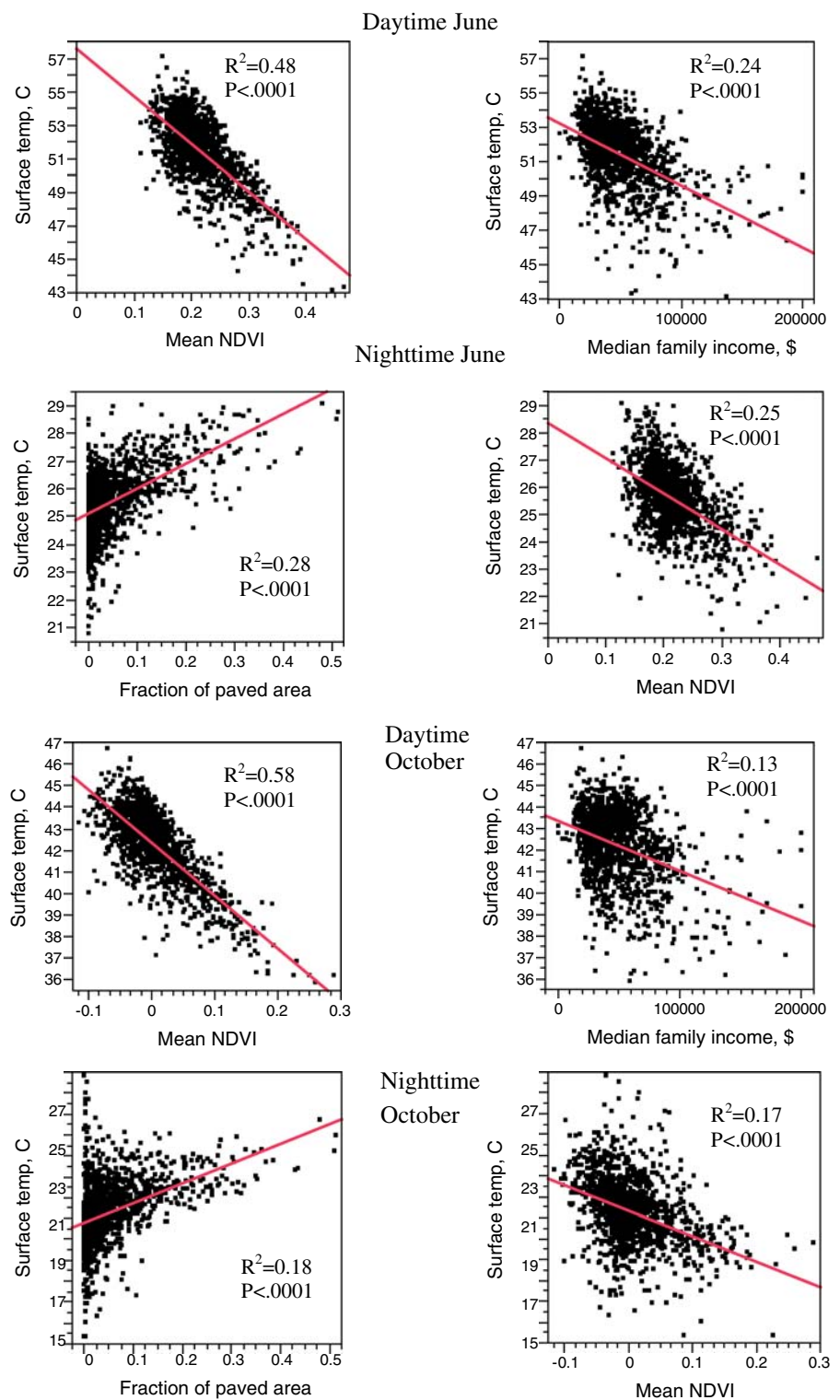
Table 2 Global OLS and GWR parameter estimates for multiple regressions constructed based on forward–backward stepwise procedures ($n = 1{,}368$)

Parameter	June daytime		June nighttime		October daytime		October nighttime	
	OLS	GWR (median)	OLS	GWR (median)	OLS	GWR (median)	OLS	GWR (median)
Intercept	75.345070	78.483558	31.529908	32.593565	54.821740	55.508733	19.914333	20.244231
NDVI	−38.927829	−41.416258	14.363006	−16.115356	−29.527550	−25.415320	−11.982573	−11.691157
PAVE	−1.888084	−3.094252	7.9201253	6.655223	−5.143126	−3.208353	8.386252	7.557833
ELEV	−0.010424	−0.010300	0.002328	0.000859	0.000281*	−0.004605	0.011660	0.014003
WAT	−21.852288	−21.781592	–	–	−24.414597	−18.977302	13.680034	5.810780
LCVAR	−0.178948	−0.185865	−0.065999	−0.023124	−0.095658	−0.117967	0.091551	0.070789
FAMINC	−0.000006	0.000002	0.000012	0.000010	−0.000004	−0.000003	0.000011	0.000009
DENSE	–	–	0.000078	0.000038	−0.000173	−0.000153	0.000027	0.000006
YBUILT	−0.000050*	−0.000281	−0.000425	−0.000246	−0.000020*	−0.000219	−0.000102*	−0.000243

NDVI = mean vegetation density within each block group (0–100%), PAVE = fraction of total area covered by pavements (0–100%), ELEV = elevation (m), WAT = fraction of total area covered by open water (0–100%), LCVAR = variability of land covers within each block group (number of land covers), FAMINC = median family income ($), DENSE = population density (persons/square km), YBUILT = median age of housing structures (year built)

* Parameter is not significant according to the t statistic for the hypothesis $\beta = 0$ ($\alpha = 0.05$)

Table 3 Regression diagnostics for both the OLS and the GWR regressions ($n = 1{,}368$)

| Regression model	Adj. R^2	SEE	AICc	F
June daytime				
Global OLS	0.586	1.226	4,450.35	
GWR	0.733	0.985	3,918.75	12.927
June nighttime				
Global OLS	0.432	0.887	3,564.25	
GWR	0.612	0.733	3,129.97	9.059
October daytime				
Global OLS	0.641	1.010	3,921.27	
GWR	0.738	0.864	3,594.50	6.552
October nighttime				
Global OLS	0.393	1.200	4,392.87	
GWR	0.767	0.744	3,187.21	25.139

patterns which often do not fit the characteristics of an idealized atmospheric UHI (Nichol 1996; Streutker 2002). Nichol (1996) argued that earlier studies (Goldreich 1985; Roth et al. 1989) detected an heat island because low-resolution data were used, whereas when high-resolution daytime data is analyzed, such island is rarely seen. Instead of a single heat island we often observe hotspots of elevated surface temperature in multiple locations of an urban area. Hence we suggest that an urban heat "archipelago" may be a

more appropriate term. Consisting of multiple cities and towns, the Phoenix metropolitan region lacks a well-developed and mature urban downtown core (Golden 2004), and its surface temperature patterns corroborate this suggestion.

We found that heterogeneity of the land-cover mosaic inside the metropolitan area entails the complexity in surface temperature spatial distributions. Surface temperature patterns (Fig. 2) are quite heterogeneous and reveal high local gradients. Importantly, intra-urban differences in surface temperature were often in the same range as or even larger than an urban–rural gradient. For example, the difference between mean nighttime surface temperature of pavements (PAVE) and urban vegetation (UVEG), the two land covers frequently found in close proximity, can be more than 9°C in June and 7°C in October. Yet, the difference was less than 8 and 6°C, respectively when PAVE was compared to Atriplex (ATR) desert (Fig. 4). Agricultural land use is another interesting example where daytime temperature differences are quite large between cooler vegetated and adjacent warmer fallow fields. At night the difference is minimized due to the faster cooling of open soil.

Paved areas are hottest urban surfaces at both day and night because they have high thermal inertia allowing them to absorb and store more sunlight

Fig. 6 Mean surface temperature predictions for 1,368 Census block groups from the global OLS and the GWR regressions
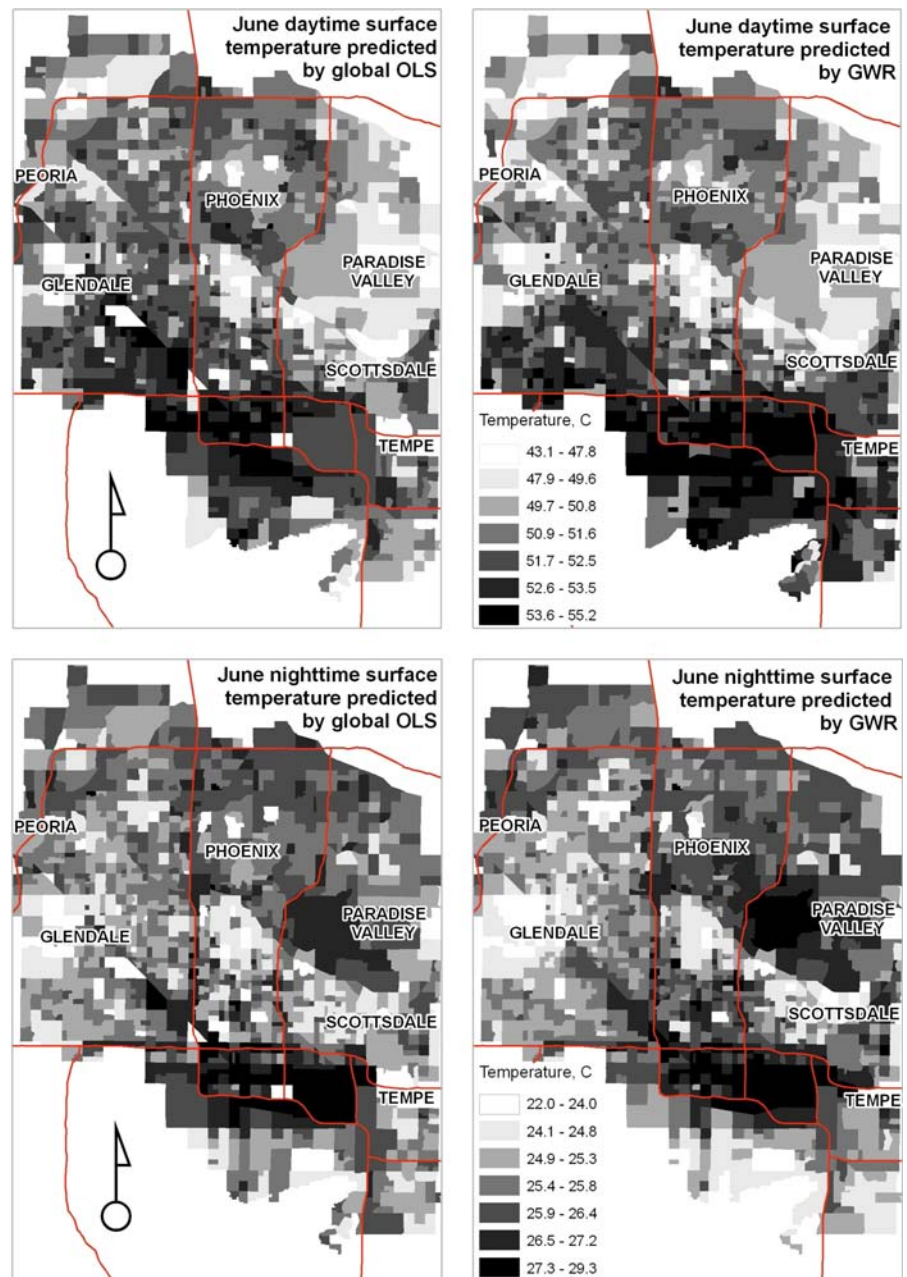

during a day which is a function of surface albedo (Taha 1997). On the other hand, irrigated vegetation cools the surroundings due to increased evapotranspiration which enhances positive latent exchange and is often referred to as an "oasis effect" (Brazel et al. 2000) (Fig. 5). Shading by dense tree canopy and presence of open water can be additional cooling factors. The UHI in Phoenix develops at night due to faster cooling of soils in the sparsely vegetated desert

but a slower release of energy accumulated in urban structures. At night, plants close their stomata and reduce latent heat exchange. This explains the significantly lower negative correlation between NDVI and nighttime surface temperature (Fig. 5). Instead, overheated paved areas become the significant positive correlate of temperature.

In summary, surface temperatures in Phoenix are characterized by considerable spatial and temporal
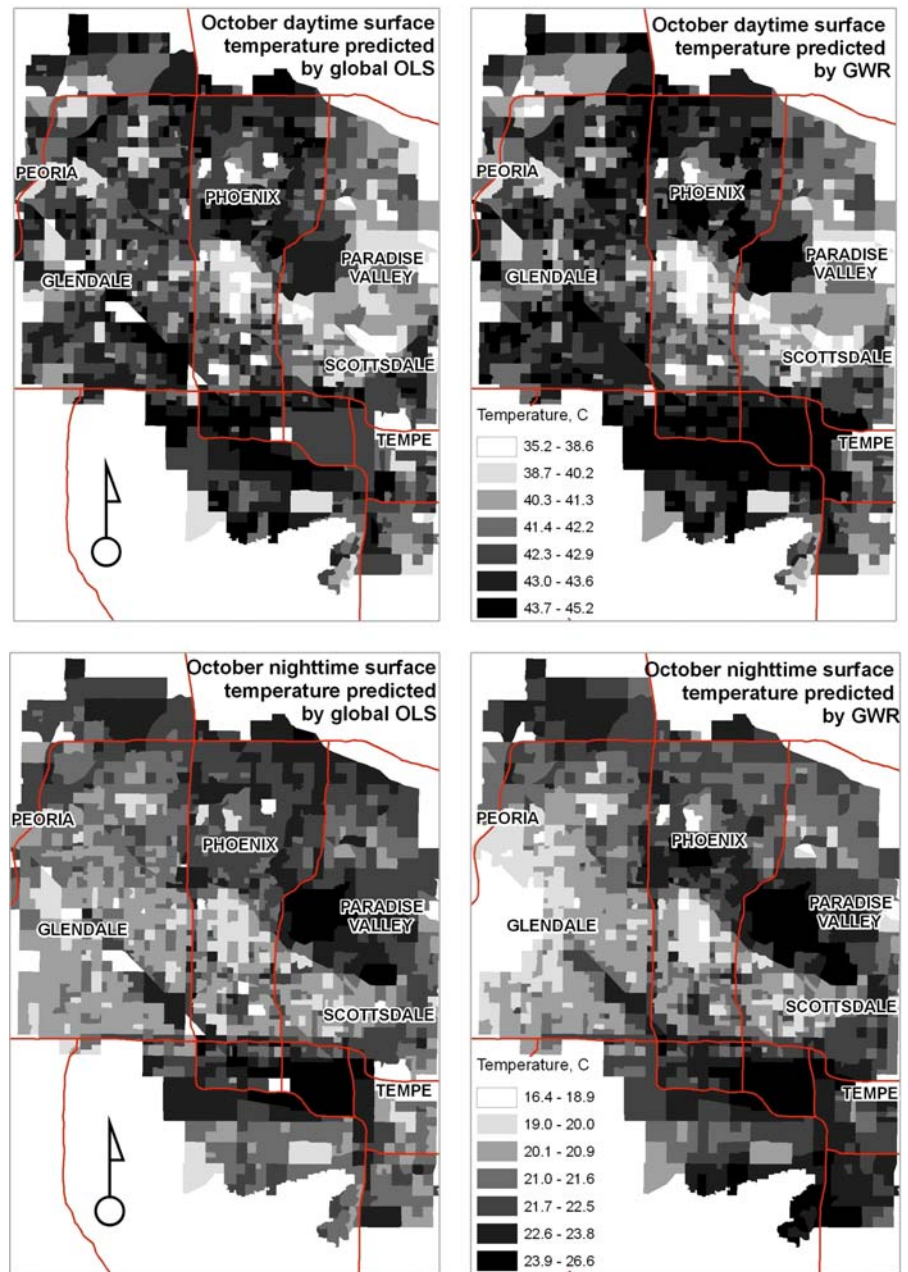
heterogeneity by forming an archipelago of SUHI at night and heat sink in the morning. Because surface temperature is uniquely related to surface properties, the use of detailed land-cover maps with relatively homogenous (at a given scale) surfaces can help in accurately quantifying temperature gradients across the entire region.

Effects of vegetation patterns and socioeconomic factors on temperature variations in the urban landscape

The relationship between NDVI and surface temperature is well established (Carlson and Arthur 2000; Gallo et al. 1993a; Gillies et al. 1997; Owen et al.

[1998a](#); [Quattrochi and Ridd 1998](#); [Sandholt et al. 2002](#); [Weng and Larson 2005](#); [Weng et al. 2004](#)), but combined effects of vegetation, buildings, pavements, and other characteristics of urban surfaces have been less explored. Our regression analyses confirmed the important role of vegetation and pavements in explaining spatio-temporal variation of temperatures in Phoenix. These variables appear as dominant drivers of surface temperature and both are effectively mediated by humans. SUHI emerges as a result of socio-economic development and affects human life in cities. It should be investigated in conjunction with analysis of socio-economic structure and dynamics ([Brazel et al. 2007](#); [Guhathakurta and Gober 2007](#); Jenerette et al. [2007](#)).

Our findings of the effect of family income levels on surface temperature are quite close to surface temperature rise by 0.28°C for every $10,000 increase found by Jenerette et al. ([2007](#)) for the entire metropolitan area, although their analysis was conducted at the coarser level of census tracts and used different but much related variable—the household income. Our results also support both the rural-to-urban hypothesis and the luxury effect hypothesis tested by Jenerette et al. ([2007](#)). In contrast with their research, we conducted analyses at the finer scale and used the expanded set of independent variables to explain temperature patterns recorded by the advanced ASTER instrument. Our findings highlight seasonal and diurnal differences in surface temperatures in Phoenix and demonstrate the varying roles of different independent variables. In particular, our results suggest that nighttime surface temperatures are less controlled by the neighborhood socio-economic status and more correlated with the areas of pavements, instead. Lastly, we employed the GWR regression which accounts for spatially varying relationships, and as such it is a more appropriate analytical framework in conducting research involving multiple spatial data layers with autocorrelated structures.

References

Arnfield AJ (2003) Two decades of urban climate research: a review of turbulence, exchanges of energy and water, and the urban heat island. Int J Climatol 23:1–26

Baker LA, Brazel AJ, Selover N et al (2002) Urbanization and warming of Phoenix (Arizona, USA): impacts, feedbacks, and mitigation. Urban Ecosyst 6:183–203

Balling RC, Brazel SW (1988) High-resolution surface temperature patterns in a complex urban terrain. Photogramm Eng Remote Sens 54:1289–1293

Balling RC, Brazel SW (1989) High-resolution nighttime temperature patterns in Phoenix. J Ariz-Nev Acad Sci 23:49–53

Bonan GB (2002) Ecological climatology: concepts and applications. Cambridge university press, Cambridge

Brazel A, Selover N, Vose R et al (2000) The tale of two climates—Baltimore and Phoenix urban LTER sites. Clim Res 15:123–135

Brazel A, Gober P, Lee SJ et al (2007) Determinants of changes in the regional urban heat island in metropolitan Phoenix (Arizona, USA) between 1990 and 2004. Clim Res 33:171–182

Carlson TN, Arthur ST (2000) The impact of land use—land cover changes due to urbanization on surface microclimate and hydrology: a satellite perspective. Global Planet Change 25:49–65

Carnahan WH, Larson RC (1990) An analysis of an urban heat sink. Remote Sens Environ 33:65–71

Fortin MJ, Dale MRT (2005) Spatial analysis: a guide for ecologists. Cambridge University Press, Cambridge

Fotheringham S, Brundson C, Charlton M (2002) Geographically weighted regression: the analysis of spatially varying relationships. Wiley, Chichester

Gallo KP, McNab AL, Karl TR et al (1993a) The use of a vegetation index for assessment of the urban heat island effect. Int J Remote Sens 14:2223–2230

Gallo KP, McNab AL, Karl TR et al (1993b) The use of NOAA AVHRR data for assessment of the urban heat island effect. J Appl Meteorol 32:899–908

Gillespie AR, Matsunaga T, Rokugawa S et al (1998) Temperature and emissivity separation from advanced spaceborne thermal emission and reflection radiometer (ASTER) images. IEEE Trans Geosci Remote Sens 36:1113–1126

Gillies RR, Cui J, Carlson TN et al (1997) A verification of the 'triangle' method for obtaining surface soil water content and energy fluxes from remote measurements of the normalized difference vegetation index (NDVI) and surface radiant temperature. Int J Remote Sens 18:3145–3166

Golden J (2004) The built environment induced urban heat island effect in rapidly urbanizing arid regions—a sustainable urban engineering complexity. Environ Sci 1:321–349

Goldreich Y (1985) The structure of the ground-level heat island in a central business district. J Appl Meteorol 24:1237–1244

Grimm N, Faeth S, Golubiewski N et al (2008) Global change and the ecology of cities. Science 319:756–760

Grimmond CSB, Oke TR (2002) Turbulent heat fluxes in urban areas: observations and a local-scale urban meteorological parameterization scheme (LUMPS). J Appl Meteorol 41:792–810

Grossman-Clarke S, Zehnder JA, Stefanov WL et al (2005) Urban modifications in a mesoscale meteorological model and the effects on near-surface variables in an arid metropolitan region. J Appl Meteorol 44:1281–1297

Guhathakurta S, Gober P (2007) The impact of the Phoenix urban heat island on residential water use. J Am Plann Assoc 73:317–329

Hafner J, Kidder SQ (1999) Urban Heat Island modeling in conjunction with satellite-derived surface/soil parameters. J Appl Meteorol 38:448–465

Hartz DA, Prashad L, Hedquist BC et al (2006) Linking satellite images and hand-held infrared thermography to observed neighborhood climate conditions. Remote Sens Environ 104:190–200

Hsu SI (1984) Variation of an urban heat island in Phoenix. Prof Geogr 36:196–200

Huete AR, Jackson RD (1987) Suitability of spectral indices for evaluating vegetation characteristics on arid rangelands. Remote Sens Environ 23:213–232

Jauregui E (1993) Mexico City's urban heat island revisited. Int J Climatol 9:169–180

Jenerette GD, Harlan SL, Brazel A et al (2007) Regional relationships between surface temperature, vegetation, and human settlement in a rapidly urbanizing ecosystem. Landscape Ecol 22:353–365

Jonsson P (2004) Vegetation as an urban climate control in the subtropical city of Gaborone, Botswana. Int J Climatol 24:1307–1322

Kato S, Yamaguchi Y (2007) Estimation of storage heat flux in an urban area using ASTER data. Remote Sens Environ 110:1–17

Kim HH (1992) Urban heat island. Int J Remote Sens 13:2319–2336

Lowry JH Jr, Ramsey RD, Boykin K et al (2005) The southwest regional gap analysis project: final report on land cover mapping methods. RS/GIS Laboratory, Utah State University, Logan (Utah. p. 50)

Lu D, Weng Q (2006) Spectral mixture analysis of ASTER images for examining the relationship between urban thermal features and biophysical descriptors in Indianapolis, Indiana, USA. Remote Sens Environ 104:157–167

Nasrallah HA, Brazel A, Balling RC Jr (1990) Analysis of the Kuwait city urban heat island. Int J Climatol 10:401–405

Neter J, Kutner MH, Nachtsheim CJ et al (1996) Applied linear statistical models. McGraw-Hill/Irwin, Boston

Nichol JE (1996) High-resolution surface temperature patterns related to urban morphology in a tropical city: a satellite-based study. J Appl Meteorol 35:135–146

Nichol JE (1998) Visualisation of urban surface temperatures derived from satellite images. Int J Remote Sens 19:1635–1637

Oke TR (1976) The distinction between canopy and boundary-layer heat islands. Atmosphere 14:268–277

Oke TR (1982) The energetic basis of the urban heat island. Quart J Royal Meteorol Soc 108:1–24

Oke TR (1997) Urban climates and global change. In: Perry A, Thompson R (eds) Applied climatology: principles and practices. Routledge, London, pp 273–287

Owen TW, Carlson TN, Gillies RR (1998a) An assessment of satellite remotely-sensed land cover parameters in quantitatively describing the climatic effect of urbanization. Int J Remote Sens 19:1663–1681

Owen TW, Carlson TN, Gillies RR (1998b) Remotely sensed surface parameters governing urban climate change. Int J Remote Sens 19:1663–1681

Pena J (2008) Relationships between remotely sensed surface parameters associated with the urban heat sink formation in Santiago, Chile. Int J Remote Sens 29:4385–4404

Quattrochi DA, Ridd MK (1998) Analysis of vegetation within a semiarid urban environment using high spatial resolution airborne thermal infrared remote sensing data. Atmos Environ 32:19–33

Roth M, Oke TR, Emery WJ (1989) Satellite-derived urban heat islands from three coastal cities and the utilization of such data in urban climatology. Int J Remote Sens 10:1699–1720

Ruddell DM, Harlan SL, Grossman-Clarke S et al (2009) Risk and exposure to extreme heat in microclimates of Phoenix, AZ. In: Showalter PS, Lu Y (eds) Geospatial techniques in urban hazard and disaster analysis. Springer, New York (in press)

Sandholt I, Rasmussen K, Andersen J (2002) A simple interpretation of the surface temperature/vegetation index space for assessment of surface moisture status. Remote Sens Environ 79:213–224

Souch C, Grimmond CSB (2006) Applied climatology: urban climate. Prog Phys Geogr 30:270–279

Spronken-Smith RA, Oke TR (1998) The thermal regime of urban parks in two cities with different summer climates. Int J Remote Sens 19:2085–2104

Stabler LB, Martin C, Brazel A (2005) Microclimates in a desert city were related to land use and vegetation index. Urban For Urban Green 3:137–147

Stefanov WL, Ramsey MS, Christensen PR (2001) Monitoring urban land cover change: an expert system approach to land cover classification of semiarid to arid urban centers. Remote Sens Environ 77:173–185

Stefanov W, Prashad L, Eisinger C et al (2004) Investigation of human modifications of landscape and climate in the Phoenix Arizona Metropolitan area using MASTER data. In: International archives of the photogrammetry, remote sensing, and spatial information sciences. ISPRS, Istanbul, Turkey, pp 1339–1347

Streutker DR (2002) A remote sensing study of the urban heat island of Houston, Texas. Int J Remote Sens 23:2595–2608

Taha H (1997) Urban climates and heat islands: albedo, evapotranspiration, and anthropogenic heat. Energy Build 25:99–103

Tucker CJ (1979) Red and photographic infrared linear combinations for monitoring vegetation. Remote Sens Environ 8:127–150

Upmanis H, Eliasson I, Lindqvist S (1998) The influence of green areas on nocturnal temperatures in a high latitude city (Göteborg, Sweden). Int J Climatol 18:681–700

Voogt JA (2002) Urban Heat Island. In: Douglas I (ed) Encyclopedia of global environmental change. Wiley, Chichester, pp 660–666

Voogt JA, Grimmond CSB (2000) Modeling surface sensible heat flux using surface radiative temperatures in a simple urban area. J Appl Meteorol 39:1679–1699

Voogt JA, Oke TR (2003) Thermal remote sensing of urban climates. Remote Sens Environ 86:370–384

Watkins R, Palmer J, Kolokotroni M (2007) Increased temperature and intensification of the urban heat island: implications for human comfort and urban design. Built Environ 33:85–96

Weng Q, Larson RC (2005) Satellite Remote Sensing of Urban Heat Islands: Current Practice and Prospects. In: Jensen RR, Gatrell JD, McLean DD (eds) Geo-spatial technologies in urban environments. Springer, Berlin, pp 91–111

Weng Q, Lu D, Schubring J (2004) Estimation of land surface temperature—vegetation abundance relationship for urban heat island studies. Remote Sens Environ 89:467–483

Wilson JS, Clay M, Martin E et al (2003) Evaluating environmental influences of zoning in urban ecosystems with remote sensing. Remote Sens Environ 86:303–321

Wu J (2008a) Making the case for landscape ecology: an effective approach to urban sustainability. Landsc J 27:41–50

Wu J (2008b) Toward a landscape ecology of cities: beyond buildings, trees, and urban forests. In: Carreiro MM, Song YC, Wu J (eds) Ecology, planning and management of urban forests: international perspectives. Springer, New York, pp 10–28

Xian G, Crane M (2006) An analysis of urban thermal characteristics and associated land cover in Tampa Bay and Las Vegas using Landsat satellite data. Remote Sens Environ 104:147–156